International Journal of Engineering & Technology, 7 (4.10) (2018) 197-201

International Journal of Engineering & Technology

Website: www.sciencepubco.com/index.php/IJET

Research paper

A Multi-Scale Framework for Bias Field Estimation in MRI Brain Images

Maryjo M George[1], Kalaivani S[2]*

[1,2]Department of Communication Engineering, School of Electronics Engineering, VIT, Vellore-632014, India
**Corresponding author E-mail: kalaivani.s@vit.ac.in*

Abstract

Intensity inhomogeneity is an artifact in MR brain images and causes intensity variation of same tissues on the basis of location of the tissue within the image. It is crucial to minimize this phenomenon to improve the accuracy of the computer-aided diagnosis. Unlike the several methods proposed in the past to minimize intensity inhomogeneity, this proposed method uses a pyramidal decomposition strategy to estimate the bias field in MR brain images. The bias field estimated from the proposed multi-scale framework can be effectively used for intensity inhomogeneity correction of the acquired MR data. The proposed methodology has been tested on simulated database and quantitative analyses in terms of coefficient of variation in grey matter and white matter tissue regions separately and combined coefficient of joint variation are assessed. The qualitative and quantitative analyses on the corrected data indicate that the method is effective for intensity inhomogeneity on brain MR images.

Keywords: *Bias field correction; Gaussian pyramid; Intensity inhomogeneity; Pyramidal decomposition; Wiener filter*

1. Introduction

MRI (Magnetic Resonance Imaging) is a widely preferred medical imaging modality to diagnose brain abnormalities as it has no harmful effects on the patient's body. Also, MRI is a non-invasive as well as a non-ionizing multi-planar medical imaging technique. But, MR images suffer from several inherent artifacts that include bias field and noise. The bias field artifact is also known as intensity inhomogeneity which alters the intensities of tissue with respect to the pixel location. This leads to overlapping of intensity levels corresponding to different tissue regions. Although this phenomenon does not have much impact on the visual diagnosis, it makes a difference when the image is used for automated analyses.

The major reason causing bias field is the non-uniformity of MR scanner RF coil sensitivity profile. Several other factors are eddy currents induced by gradient coils and patient's susceptibility and position in the scanner [1]. The various techniques that have been adopted to minimize the intensity inhomogeneity can be broadly classified into two types: prospective and retrospective. The Prospective techniques deal with calibration of the hardware and enhancement in the acquisition process. For example, oil or water phantoms with priori known physical characteristics can be used for bias field estimation in a scanner [2]. Images from multiple coils such as surface and body coils could be utilized to achieve intensity homogeneous and high SNR images [3]. Special sequences are also introduced specifically to reduce the effect of bias field [4]. Retrospective techniques deal with the acquired MRI and mainly categorized into filtering, segmentation, surface fitting and histogram based methods.

Homomorphic unsharp masking [5] and homomorphic filtering [6] are the main techniques in filtering category where a low pass filter is utilized to extract the bias field. Segmentation and bias field correction could be benefited from each other as segmented regions are considered to have uniform intensity. Expectation-maximization [7], Fuzzy c-means [8], nonparametric segmentation incorporating spatial information on multispectral images [9] and non-parametric maxshift [10] are the preferred segmentation strategies in this method. Surface fitting methods [11] represent bias field as a parametric surface using a spline or polynomial. The state-of-art method, N4 [12] is a histogram based method which estimates the field that exploits high frequency content in the input image histogram.

Multi-scale frameworks for estimation of bias field are proved to be effective [13]. The methodology proposed in this paper processes the decomposed Gaussian pyramid levels of the input MR image to approximate the bias field. This is a non-iterative strategy and doesn't involve any prior knowledge on the scanner or patient. The bias field modulated MR image can be corrected by using the obtained approximation of bias field. The paper is systematized as follows: Section 2 details the related work; section 3 deals with the method for estimating the bias field. The results obtained on simulated database are provided in results section followed by conclusion from quantitative analyses.

2. Related work

2.1. Gaussian Pyramids

Gaussian pyramid is a means to represent an image at various resolutions in a hierarchical manner [14]. The image is decomposed at multiple scales by recursive convolution with a Gaussian filter along with down sampling.

At the initial level, a decomposed image of same size as the original image is obtained and consecutive rows and columns of the level image are removed for down sampling. At each level the size of the image reduces to half of its previous level. The next decomposed level is obtained by spatial convolution with the same

Gaussian kernel. Fig. 1 shows an example of a Gaussian pyramidal decomposition of an image. Generally, the Gaussian kernel is taken either as a low-pass filter or a band-pass filter. In case of a low-pass filter, the higher levels are completely smoothened versions of the input image at reduced resolutions.

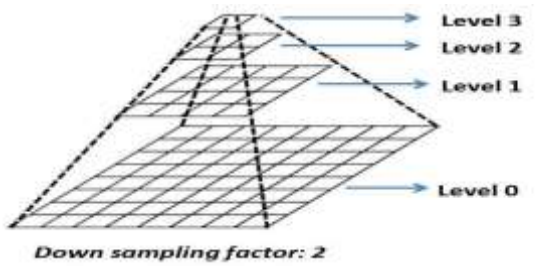

Fig. 1: Gaussian pyramidal decomposition of an 8x8 image.

3. Methodology

It is assumed that product of true image and bias field together with additive noise constitute the acquired input MR image. The bias field modulated MR image can be represented by (1):

$$O(a, b) = T(a, b)\, S(a, b) + \gamma \quad (1)$$

Where observed tissue intensity at a particular location (a, b) is denoted by O(a, b). The true intensity level and bias field at the same location are denoted by T(a, b) and S(a, b). The inherent noise in the acquired image is presumed to follow a Rician distribution that is denoted by γ.

As bias field follows a low frequency nature and the acquired image can be considered as a low-frequency modulated 2D signal [1]. The acquired image is decomposed into multi scale representation using a Gaussian pyramidal decomposition. At a suitable decomposed level, the contrast in the input image is superior compared to the acquired image and the bias field can be estimated from this decomposed level of the pyramid after necessary processing. Level 1 is found to be suitable for T1w, T2w and PD modality images from qualitative analysis. The proposed multi-scale methodology is described in Fig. 2.

3.1. Pre-Processing

The cerebro-spinal fluid tissues surrounded by grey matter in the brain MR image correspond to higher frequency and thus are eliminated using morphological filling operation [15]. The cerebro-spinal tissue pixels enclosed by grey matter can be considered as regional minima or maxima that are disconnected from a region boundary. Hence, by filling the small regions of cerebro-spinal fluid with grey matter tissue intensity reduces the total intensity variations in the image. Therefore, morphological hole-filling operation is carried out in the input image as a pre-processing stage.

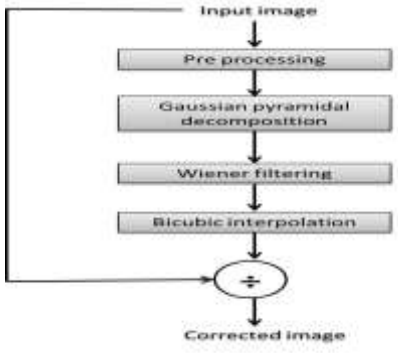

Fig. 2: Proposed multi-scale framework for MRI bias field correction

3.2. Gaussian Pyramidal Decomposition

The bias field degraded image is decomposed at different scales using a Gaussian pyramid. At each level, the image is convolved with a Gaussian blur and is scaled down to half of the resolution as follows.

$$M_l(p, q) = \sum_m \sum_n g(m, n)\, M_{l-1}(2p+m, 2q+n) \quad (2)$$

Where, g(m, n) represents the Gaussian weight and M_l denotes the decomposed image at l^{th} level. The Gaussian kernel of size 5x5 is formulated as below where α is the kernel center weight and is taken as 0.375. G is the Kroncker tensor product of K^{1D} and its transpose.

$$K^{1D} = \left[\, 0.25 - \alpha/2 \quad 0.25 \quad \alpha \quad 0.25 \quad 0.25 - \alpha/2 \,\right] \quad (3)$$

$$G = \mathrm{kron}\left(K^{1D}, K^{1D^T}\right) \quad (4)$$

The first level is utilized here as contrast between tissue regions is more than the actual image compared to the other levels. Therefore, the bias field can be easily extracted from this level. The first level is a low pass filtered form of the input image but still contains edges of tissue regions. A smoothing operation is required on this decomposed level in order to approximate the same to the actual slowly varying bias field.

3.3. Wiener Filtering

Wiener filter [16] acts as a low-pass filter in this case to smooth the first decomposed level from the Gaussian pyramid. The filter estimates the local mean μ_R and variance σ^2_R of a region, R of specified size as follows.

$$\mu_R = \frac{1}{PQ} \sum_{x,\, y \in R} O(x, y) \quad (5)$$

$$\sigma^2_R = \frac{1}{PQ} \sum_{x,\, y \in R} \left(O(x, y) - \mu_R\right)^2 \quad (6)$$

$$w(x, y) = \mu_R + \frac{\sigma^2_R - T}{\sigma^2_R} \left(O(x, y) - \mu_R\right) \quad (7)$$

Where, T represents the noise variance in the region. The noise variance is not explicitly provided for the execution. Therefore, the average of region variances is assumed to be the noise variance. An adaptive pixel-wise filtering is performed depending upon the neighborhood statics. The wiener filtering here acts as a smoothing approach. The high frequency contents corresponding to the rapidly varying edges are smoothened to produce a slowly varying 2D surface. The surface obtained can be approximated as the bias field at a lower resolution. An interpolation method is required for higher resolution approximation of the bias field.

3.4. BICUBIC Interpolation

The bias field obtained after wiener filtering is the processed version of first level Gaussian pyramid decomposition. The Gaussian pyramidal decomposition at the first level is of half resolution of the acquired image and resizing the image to its original size requires an interpolation technique. The bias field is considered to be of non-linear nature. Therefore, in order to better represent the smoothly varying bias field, a bicubic interpolation [17] is preferred. The interpolation function is a third order polynomial which is piece-wise continuous over a region. The region of size 4x4 is considered here for interpolation. The interpolated surface is smoother than the low resolution image and the properties of bicubic interpolation causes minimum interpolation artifacts. The

interpolated intensity from a 4x4 region can be estimated as follows.

$$D(u, v) = \sum_{i=1}^{4} \sum_{j=1}^{4} c_{ij} u^i v^j \quad (8)$$

Where, the coefficients $\{c_{ij}\}$ can be found by solving equations obtained by matching known intensity values at the 4x4 region, from first order derivatives along x and y directions separately and cross derivatives along x and y.
The final bias field is the union of such interpolated sub regions as given in (9). The interpolated sub regions are continuous and its derivative is also continuous.

$$\hat{S} = \bigcup D \quad (9)$$

The input image can be corrected from bias field estimate using (10). The corrected image is found as follows by pixel wise division of the input image and estimated bias field, $\hat{S}$:

$$\hat{T}(a, b) = O(a, b) / \hat{S}(a, b) \quad (10)$$

4. Results and Discussion

The proposed frame work has been tested on BrainWeb simulated database [18] for T1w, T2w and PD volumes of size 181x217x181. The slice thickness was 1mm. The ground truth bias fields were available in the database. For T1w, T2w and PD images, bias fields labeled as field A, field B and field C were applied respectively in levels of 20% and 40%. And Rician distribution noise of 1%, 3% and 5% were considered in the signal regions. Slices with more than 2000 brain pixels were only considered for the application of proposed framework. The simulations were performed on a windows platform system with 4Gb RAM and Pentium(R) dual-core 2.2GHz processor. The average time taken for the execution of the proposed method on a volume in the experiment was 20 ± 05 sec.

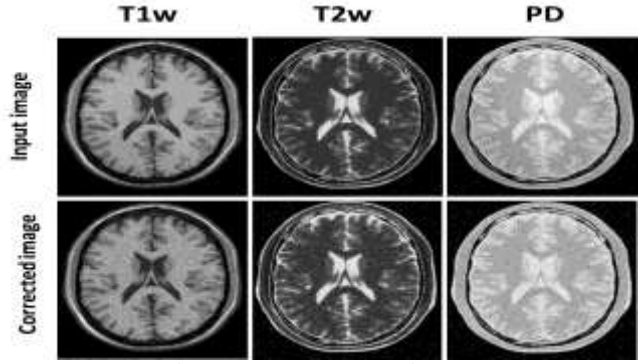

Fig. 3: First row (left to right): Input image of T1w, T2w and PD (5% noise level, 40% bias field). Second row (left to right): Corrected image of T1w, T2w and PD.

The results obtained after application of the proposed methodology on T1w, T2w and PD images from the BrainWeb dataset are shown in Fig. 3. The first row of Fig. 3 shows T1w, T2w and PD axial mid-slice images which are degraded by 5% noise level and 40% bias field. The corrected images obtained after the application of the proposed methodology on these input images are shown in the second row of Fig. 3. The removal of intensity inhomogeneity in all the three modalities is evident from this figure.
The results obtained after the processing stage on the T1w axial image shown in Fig. 3 is provided in Fig. 4. Fig. 4.b displays the result of hole-filling process executed on Fig. 4.a. The morphological hole filling method performed on the input image, Fig. 4.a has replaced the cerebro-spinal fluid tissues with grey matter tissue intensity. The strong edges present in the input images are diminished in Fig. 4.b through morphological filling operation.

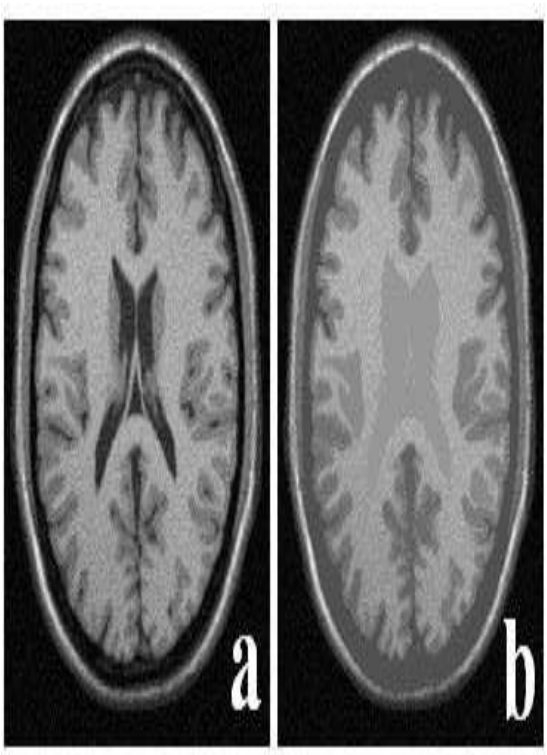

Fig. 4: [a] T1w axial input image **[b]** Pre-processed image

The image obtained after hole-filling operation was decomposed using Gaussian pyramids into three levels as shown in Fig. 5. The level 0 represents the actual image and the level 1 is a low-pass filtered form of the actual input image. The size of the decomposed image has been considerably reduced in level 2. The improvement in the contrast between different tissue regions in level 1 is clearly visible in Fig. 5.

Table 1: Coefficient of variation in white matter and grey matter regions WM: White matter, GM: Grey matter

		Noise level (%)	1		3		5	
		Bias field (%)	20	40	20	40	20	40
T1w	**GM**	Input	9.03±.98	10.05±.73	10.07±.90	10.98±.71	11.21±.56	12.12±.61
		Corrected	8.95±.81	9.71±.62	9.79±.89	9.91±.62	10.89±.42	11.97±.71
	WM	Input	4.21±.15	10.01±.99	5.45±.67	6.17±.24	6.78±.15	7.18±.47
		Corrected	4.16±.08	9.76±.83	5.02±.88	5.98±.54	6.72±.54	7.09±.61
T2w	**GM**	Input	16.75±1.98	16.98±.68	17.32±.58	18.99±.69	20.11±.55	22.14±.29
		Corrected	14.68±1.81	13.95±.32	15.28±.09	17.91±.99	18.09±.15	20.12±.96
	WM	Input	7.12±.91	7.19±.80	11.78±.94	14.01±.84	17.05±.99	20.32±1.01
		Corrected	7.09±.62	7.16±.68	10.73±.49	12.00±.41	16.02±.91	18.29±.91
PD	**GM**	Input	3.91±.73	5.71 ±1.23	5.09±.26	6.43±1.11	8.41±.94	10.56±1.34
		Corrected	3.24±.31	5.29 ±.99	6.69±.45	5.98±.99	6.02±.29	9.21±1.67
	WM	Input	3.59±.51	6.89±.90	5.01±.26	6.09±1.10	7.18±.79	10.79±1.06
		Corrected	3.02±.10	6.01±.34	6.82±.45	5.69±.83	6.80±.21	8.02±.94

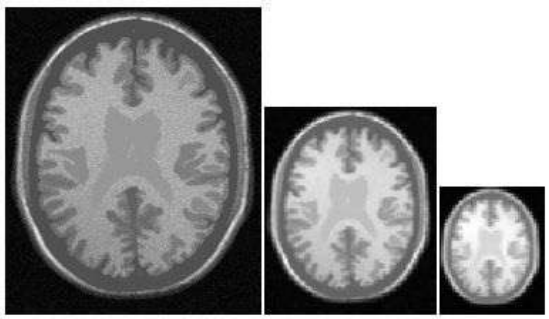

Fig. 5: Gaussian pyramidal decomposition of pre-processed image (From left to right) Level 0, Level 1and Level 2

Fig. 6.b shows the level 1 decomposed image smoothened using a wiener filter to approximate the varying bias field. The adaptive pixel-wise filtering is performed on Fig. 6.a based on the 40x40 neighborhood statics. The image obtained after the adaptive filtering is smoothly varying and is considered as the estimate of the bias field present in the input image. Fig. 6.c represents the bicubic interpolation performed on Fig. 6.b in order to resize the estimated bias to the actual input image size. Fig. 6.c is the estimated bias field present in the input image shown in Fig. 4.a. The bias field corrected image is obtained from input image and the estimated bias field by applying (10).

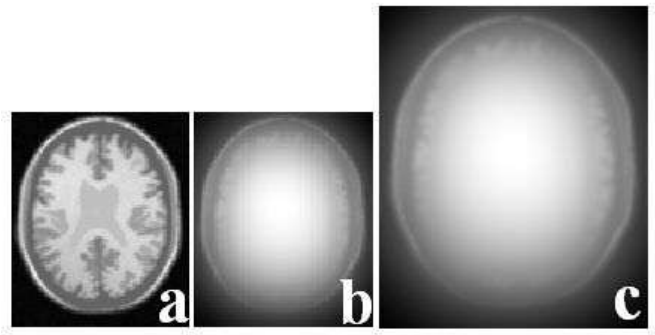

Fig. 6: [a] The Level 1 decomposition **[b]** Wiener filtered image **[c]** The estimated bias field

The quantitative analyses were performed in the corrected images to examine the efficacy of the proposed methodology. Coefficient of variation (CV) in grey matter, white matter regions is calculated according to (11) where σ and μ represent the mean and variance of a region, R. The CV values on both the tissue regions are tabulated in Table 1 for T1w, T2w and PD volumes. The ground truth segmentations used for CV calculation were available in the dataset.

$$CV(R) = \frac{\sigma(R)}{\mu(R)} \tag{11}$$

Coefficient of variation in the tissue regions is only a measure of intra-class intensity variation. Coefficient of joint variation (CJV) is calculated as provided in (12) in addition to estimate the extent of intensity overlap reduction between grey matter and white matter. CJV provides a measure of inter-class intensity variation. A good bias field correction algorithm is estimated to reduce both CV and CJV values after correction.

$$CJV(R_0, R_1) = \frac{\sigma(R_0) + \sigma(R_1)}{|\mu(R_0) - \mu(R_1)|} \tag{12}$$

The CV values obtained before and after the bias field correction on images simulated under 1%, 3% and 5% Rician noise for different modalities are tabulated in Table 1. From Table 1, it is observed that the coefficient of variation is reduced in white matter and grey matter tissue regions in all the modalities. The reduction in CV values is consistent even at higher noise levels.

The CJV values for the same set of images are provided in Table 2. The improvement in the contrast between white matter and grey matter regions after correction can be explained through the reduction in CJV values as shown in Table 2. The considerable decrease in the CJV values after the application of the proposed methodology indicates the improved separation in inter-class region intensities. This implies the proposed methodology is effective towards intensity inhomogeneity in T1w, T2w and PD modality images.

Table 2: Coefficient of joint variation

	Noise level (%)	1		3		5	
	Bias field (%)	20	40	20	40	20	40
T1w	Input	0.48 ±0.70	0.50±0.23	0.53±0.35	0.65±0.81	0.71 ±0.22	0.81 ±0.93
	Corrected	0.46±0.07	0.48±0.51	0.51±0.54	0.62±0.74	0.69±0.16	0.78±0.02
T2w	Input	0.74±0.67	0.76±0.40	0.87±0.47	0.90 ±0.32	0.99±0.62	1.02±0.69
	Corrected	0.72±0.83	0.73±0.05	0.86 ±0.41	0.88 ±0.63	0.97±0.91	0.99±0.88
PD	Input	0.62±0.09	0.75±0.56	0.82±0.50	0.98±0.77	1.03±0.52	1.99±0.37
	Corrected	0.59±0.01	0.71±0.32	0.79 ±0.99	0.96±0.04	0.98±0.47	1.96±0.72

5. Conclusion

The paper presents a multi-scale decomposition frame work for bias field correction in brain MR images. Bias field present in an acquired MRI can be estimated from a low-pass filtered form of the same. The multi-scale decomposition of the input image is obtained using Gaussian pyramids. Level 1 of the decomposed image is utilized to approximate the bias field with necessary smoothing operation. The estimated bias field is later utilized to correct the intensity inhomogeneity in the input image. The effectiveness of the proposed technique for removal of the bias field in T1w, T2w and PD MR brain modalities is validated qualitatively and quantitatively through visual analysis and CV and CJV values. The reduction in both CV, CJV values indicate improved homogeneity in the tissue level intensities and reduced inter-class intensity overlapping. The method is found to be more effective on PD images compared to T1w and T2w. The algorithm sustains consistency in the performance even at higher noise levels.

References

[1] Vovk, U., Pernus, F. and Likar, B. (2007), A Review of Methods for Correction of Intensity Inhomogeneity in MRI. *IEEE Transactions on Medical Imaging* 26(3), 405–421.

[2] Simmons, A., Tofts, P. S., Barker, G. J. and Arridge, S. R. (1994), Sources of intensity nonuniformity in spin echo images at 1.5 T. *Magnetic Resonance in Medicine* 32(1), 121–128.

[3] Narayana, P. A., Brey, W. W., Kulkarni, M. V. and Sievenpiper, C. L. (1988),Compensation for surface coil sensitivity variation in

magnetic resonance imaging. *Magnetic Resonance Imaging* 6(3), 271–274.
[4] Mihara, H., Iriguchi, N. and Ueno, S. (1998), A method of RF inhomogeneity correction in MR imaging. *Magnetic Resonance Materials in Physics, Biology and Medicine* 7(2), 115–120.
[5] Brinkmann, B. H., Manduca, A. and Robb, R. A. (1998), Optimized homomorphic unsharp masking for MR grayscale inhomogeneity correction. *IEEE Transactions on Medical Imaging* 17(2), 161–171.
[6] Lewis, E. B. and Fox, N. C. (2004), Correction of differential intensity inhomogeneity in longitudinal MR images. *NeuroImage* 23(1), 75–83.
[7] George, M. M. and Kalaivani, S. (2017), Intensity inhomogeneity correction and tissue segmentation of MR images: A parametric approach. *International Journal of Pure and Applied Mathematics* 115(9), 409–416.
[8] Bezdek, J. C., Hall, L. O. and Clarke, L. P. (1993), Review of MR image segmentation techniques using pattern recognition. *Medical Physics* 20(4),1033–1048.
[9] Derganc, J., Likar, B. and Pernus, F. (2002), Nonparametric segmentation of multispectral MR images incorporating spatial and intensity information. *International Society for Optics and Photonics* 391
[10] Likar, B., Derganc, J. (2002), Segmentation-based retrospective correction of intensity nonuniformity in multispectral MR images. *SPIE Medical Imaging*, 4684, 1531-1540, http://dx.doi.org/10.1117/12.467120.
[11] Dawant, B. M., Zijdenbos, A. P. and Margolin, R. A. (1993), Correction of intensity variations in MR images for computer-aided tissue classification. *IEEE Transactions on Medical Imaging* 12(4),770–781.
[12] Tustison, N. J., Avants, B. B., Cook, P. A., Yuanjie Zheng, Y., Egan, A., Yushkevich, P. A. and Gee, J. C. (2010), N4ITK: Improved N3 Bias Correction. *IEEE Transactions on Medical Imaging* 29(6), 1310–1320.
[13] George, M. M., Kalaivani, S. and Sudhakar, M. S. (2017), A non-iterative multi-scale approach for intensity inhomogeneity correction in MRI. *Magnetic Resonance Imaging* 42, 43–59.
[14] Adelson, E. H., Anderson, C H, Bergen, J. R., Burt, P J and Ogden, J M (1984), Pyramid methods in image processing. *RCA Engineer* 29 (6), 33–41.
[15] Maragos, P. (1987), Tutorial On Advances In Morphological Image Processing And Analysis. *Optical Engineering*. *International Society for Optics and Photonics*, 26(7), 267623.
[16] Kazubek, M. (2003),Wavelet domain image denoising by thresholding and Wiener filtering. *IEEE Signal Processing Letters* 10(11), 324–326.
[17] Keys, R. (1981), Cubic convolution interpolation for digital image processing. *IEEE Transactions on Acoustics, Speech, and Signal Processing* 29(6),1153–1160.
[18] Cocosco, C. A., Cocosco, C. A., Kollokian, V., Kwan, R. K.-S., Pike, G. B. and Evans, A. C. (1997), BrainWeb: Online Interface to a 3D MRI Simulated Brain Database. *Neuroimage* 5, 425.